



Cite this: *Inorg. Chem. Front.*, 2022, **9**, 5788

Nanocage-based $\{In_2Tm_2\}$ -organic framework for efficiently catalyzing the cycloaddition reaction of CO_2 with epoxides and Knoevenagel condensation†

Hongxiao Lv, Hongtai Chen, Tuoping Hu and Xiutang Zhang *

High density active sites and chemical stability for prepared MOFs are the prerequisites for their industrial applications, which prompted us to synthesize cluster-based metal–organic compounds. The combination of $[In_2Tm_2(\mu_2-OH)_2(CO_2)_{10}(H_2O)_2]$ clusters ($\{In_2Tm_2\}$) and the functional ligand 2,6-bis(2,4-dicarboxylphenyl)-4-(4-carboxylphenyl)pyridine (H_5BDCP) produced an extremely stable nanoporous skeleton of $\{(Me_2NH_2)_2[In_2Tm_2(BDCP)_2(\mu_2-OH)_2(H_2O)_2] \cdot 2DMF \cdot 3H_2O\}_n$ (**NUC-56**), whose inner surface is functionalized by Lewis acidic and basic groups of metal centers, μ_2-OH groups and $N_{pyridine}$ atoms. To the best of our knowledge, **NUC-56** is a rarely reported planar-cluster-based $\{In_2Ln_2\}$ -organic framework, which possesses an excellent confined pore environment with high porosity, large specific surface area and abundant co-existing Lewis acid and base sites. Consequently, **NUC-56a** exhibited a good catalytic performance for the cycloaddition reaction of various epoxides with CO_2 and the Knoevenagel condensation reaction of different aldehydes and malononitrile under mild conditions. Therefore, this study can provide some guidance for the precise design of practical MOFs with excellent catalytic, stability and regeneration performances through the participation of rare earth ions.

Received 16th June 2022,
Accepted 13th September 2022

DOI: 10.1039/d2qi01271e

rs.c.li/frontiers-inorganic

Introduction

Metal organic frameworks (MOFs), as a new type of porous inorganic–organic hybrid crystalline materials constructed from the exquisite combination of metal ions/clusters and diverse organic ligands, have attracted tremendous attention due to their desirable structural properties including adjustable pore size, high porosity, multiple active sites, and tailorable architectures, which have led to a wide range of applications, such as gas adsorption and separation, fluorescence sensing and heterogeneous catalysis.^{1–7} To date, there are relatively few reports on the applications of heterometallic frameworks due to the lack of mature synthetic regulation strategies. However, it has been proven that the introduction of a second metal ion in the framework is a valuable project to enhance the gas capture capacity and catalytic performance of MOFs because of the synergistic effect of two metal ions in the absence of specific mechanism processes.^{8–10} Therefore, the self-assembly of heterometallic MOFs with microchannels and extremely

exposed active sites is particularly challenging, but can be achieved by carefully designing organic ligands, reasonably configuring different metal ions and finely controlling the growth environment.^{11,12}

In addition, with the continuous expansion of industrial production and excessive use of fossil fuels, carbon dioxide (CO_2) emissions have increased at a rate of 4% per year, resulting in serious air pollution and greenhouse effect.^{13–19} However, from the perspective of resource utilization, CO_2 serves as one of the richest C1 resources on Earth with the advantages of large reserves, safety, non-toxicity and low price. Thus, converting CO_2 into valuable chemicals has strategic significance of environmental friendliness and sustainability.^{20–23} Accordingly, it is significant for the sustainable development of society to implement strategies of CO_2 capture and storage/sequestration (CCS), which have prompted the innovative preparation of functional microporous MOF-based materials.^{24–26} At present, the method for the preparation of cyclic carbonates by cycloaddition reaction using CO_2 and epoxides is consistent with the concept of “green preparation theory” and “atomic economy principle”. Also, carbonate products are widely used in lithium battery electrolytes, textiles, chemical industry, pharmaceuticals and preparation of functional polymers because of their excellent properties including high boiling point and solubility, low toxicity and

Department of Chemistry, College of Science, North University of China, Taiyuan 030051, People's Republic of China. E-mail: xiutangzhang@163.com

† Electronic supplementary information (ESI) available. CCDC 2168334. For ESI and crystallographic data in CIF or other electronic format see DOI: <https://doi.org/10.1039/d2qi01271e>

degradability.^{27–29} Nevertheless, owing to the thermodynamic stability of CO₂, cycloaddition reactions usually demand a high reaction temperature and pressure. Thus, to overcome this disadvantageous problem, various homogeneous and heterogeneous catalysts have been developed to drive the reaction process. Among them, homogeneous catalysts have some drawbacks, such as difficult separation between catalyst and product, high energy consumption, and poor economic performance.^{30–32} Therefore, based on the above-mentioned problems, a variety of heterogeneous catalysts (ionic liquids, carrier solids, metal complexes, *etc.*) have been developed. However, solid heterogeneous catalysts usually need harsh conditions because they lack accessible surface area and exposed active sites to fully activate CO₂ molecules. Thus, it is of great significance to explore innovative heterogeneous catalysts with excellent stability, cyclic performance, and high activity to promote the reaction under mild conditions.^{33–36} Thus far, MOFs have been widely used in the field of heterogeneous catalysis due to their permanent porosity, adjustable pore structure, large specific surface area, multiple reaction active sites and excellent ability to adsorb CO₂.^{37–41} In-MOFs account for a small proportion of the reported MOFs although they are based on the most common SBUs, for instance, [In(CO₂)_n], [In₃O(CO₂)_n(OH₂)_n], and [In(O/OH)]_n and sporadic heterometallic clusters of {InM₂}, {In₂M₂}, {In₃Ln}, and {In₃Ln₂}.^{42–50} Nevertheless, the outstanding catalytic performance from the high-level p-orbitals of the In³⁺ ion provides motivation for scientists to pursue a superior indium-organic frame. In addition, Ln-MOFs have attracted increasing attention because of their high chemical stability and catalytic ability for most organic reactions, which should be attributed to the powerful positive charge of Ln^{III} cations and abundant vacant electron orbitals.^{51,52} However, promising heterometallic MOFs based on the combination of rare earth ions and In³⁺ ions are rarely reported.

In view of the considerations discussed above, the multifunctional ligand of 2,6-bis(2,4-dicarboxylphenyl)-4-(4-carboxylphenyl)pyridine (H₅BDCP) was reacted with In³⁺ and Tm³⁺ for the successful synthesis of a highly stable channel-based heterometallic {In₂Tm₂}-organic framework of {[In₂Tm₂(BDCP)₂(μ₂-OH)₂(H₂O)₂·2DMF·3H₂O]_n (NUC-56) with excellent water resistance, thermal stability and a series of structural advantages, which rendered it an outstanding heterogeneous catalyst to boost cycloaddition reactions. Moreover, it also simultaneously exhibited efficient catalytic ability in the Knoevenagel condensation of aldehydes and malononitrile.

Experimental

Preparation of NUC-56 and NUC-56a

A sample of Tm₂O₃ (0.10 mmol), In(NO₃)₃·5H₂O (0.10 mmol) and H₅BDCP (0.08 mmol) in 10 mL solvent of DMF and H₂O (v:v = 8:2) with one drop of concentrated HNO₃ was heated in a Teflon-lined stainless-steel vessel at 110 °C for 2 days. The

cube crystals were collected by filtration after cooling, and the yield of crystals based on the H₅BDCP ligand was 53%. Anal. calcd for NUC-56 (C₄₀H₂₆N₃O₁₇InTm): C, 24.64; H, 2.36; N, 3.81 (%). Found: C, 24.60; H, 2.40; N, 3.77 (%). FT-IR (KBr pellet, cm⁻¹, Fig. S3†): 3750 (m), 2923 (w), 1857 (w), 1552 (w), 1500 (m), 1469 (m), 1415 (s), 1456 (s), 1089 (vs), 1014 (s), 921 (m), 858 (s), 819 (s), 777 (vs), 682 (m), 657 (m).

Results and discussion

Crystal structure description

Single-crystal X-ray diffraction analysis showed that NUC-56 crystallizes in a monoclinic system with the *C2/m* space group and exhibits a microporous three-dimensional framework of {[In₂Tm₂(BDCP)₂(μ₂-OH)₂(H₂O)₂·4DMF·3H₂O]_n with coplanar [In₂Tm₂(μ₂-OH)₂(CO₂)₁₀(H₂O)₂] clusters as the basic building units (Fig. 1a and Fig. S1†). Astonishingly, NUC-56 is a planar-cluster-based {In₂Ln₂}-organic framework, whose inner surface is functionalized by abundant coexisting Lewis acid–base sites of In³⁺, Tm³⁺, μ₂-OH and N_{pyridine} atoms. Moreover, it is noteworthy that the {In₂Tm₂} clusters exist in a coplanar configuration and NUC-56 is synthesized by the structurally oriented ligand of BDCP⁵⁻, forming a highly distorted connection mode, which resulted in the maximum exposure of the open metal sites of In³⁺ and Tm³⁺ and μ₂-OH. Therefore, the successful construction of NUC-56 offers a valuable technique for the synthesis of deeply functionalized common In-MOFs by introducing rare earth ions, which potentially have wider applicability in various catalysis fields.

Regarding the detailed internal links in NUC-56, there is a half Tm³⁺ ion, a half In³⁺ ion, a half BDCP⁵⁻, two half μ₂-OH and two half associated H₂O in the asymmetric unit. The Tm(1) and In(1) ions are firstly bridged by two μ₂-η¹:η¹ α-carboxyl groups from two phenyl rings arranged on the 2- and 6-position of pyridine in one BDCP⁵⁻ to form a binuclear unit of [InTm(CO₂)₂] (Fig. 1a), which are further connected by one μ₂-OH group, leaving a unit of [InTm(μ₂-OH)(CO₂)₂]. Also, *via* the symmetry extension, two [InTm(μ₂-OH)(CO₂)₂] units are each bridged by four μ₂-η¹:η¹ γ-carboxyl groups from four phenyl rings arranged on the 2- and/or 6-position of pyridine of the BDCP⁵⁻ ligand to form a 2D layer with the initial quadrangular [In₂Tm₂(μ₂-OH)₂(CO₂)₈(H₂O)₂] clusters as nodes, in which each adjacent Tm³⁺ and In³⁺ are bridged by two μ₂-η¹:η¹ carboxyl groups, and each In³⁺ is saturated by one associated water molecule. Furthermore, each Tm³⁺ ion in the [In₂Tm₂(μ₂-OH)₂(CO₂)₈(H₂O)₂] SBU is further cheated by one γ-carboxyl group on the 4-position of the phenyl ring from the upper and lower planes to form a 3D anionic skeleton with the formation of a complete cluster of [In₂Tm₂(μ₂-OH)₂(CO₂)₁₀(H₂O)₂] (Fig. 1d). In conclusion, each tetranuclear heterometallic {In₂Tm₂} cluster is supported by ten carboxyl groups from eight deprotonated BDCP⁵⁻ linkers. It is worth mentioning that the eight {In₂Tm₂} clusters are each woven together to generate elliptical nanocages (aperture *ca.* 14.1 Å) (Fig. 1c) with their functionalized inner surface decorated by the coex-

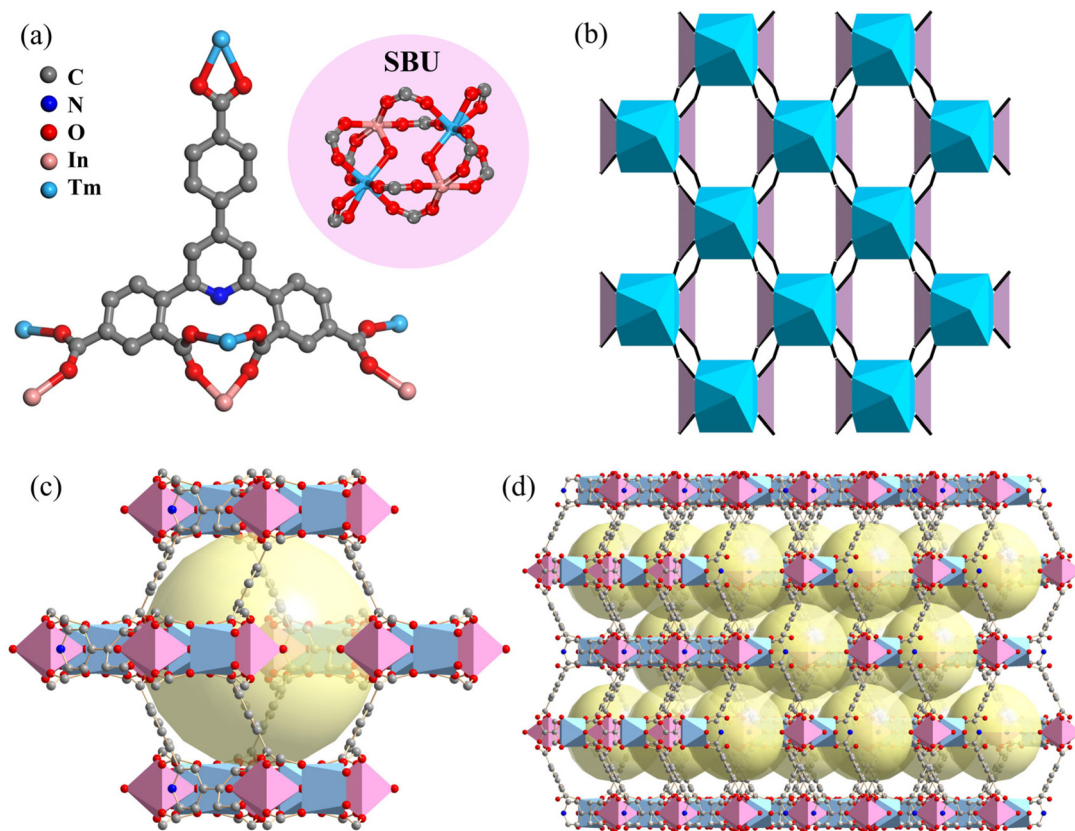


Fig. 1 Coplanar $[\text{In}_2\text{Tm}_2(\mu_2\text{-OH})_2(\text{CO}_2)_{10}(\text{H}_2\text{O})_2]$ cluster and the coordination environment of BDCP^{5-} ligand (a). Topology network with the Schläfli symbol of $\{4^{12}\cdot 6^{12}\cdot 8^4\}\{4^6\}_2$ of **NUC-56** (b). $\{\text{In}_2\text{Tm}_2\}$ cluster-shaped nanocage of **NUC-56** (c). 3D framework of **NUC-56** featured by oval nanocages (d).

isting Lewis acid and base sites. Besides, the H_5BDCP ligand has the two unique advantages, *i.e.*, spatial self-regulation and metal-cluster-orientation. Because the triaxial angle-adjustable planar H_5BDCP ligand enables three carboxylphenyl groups to rotate freely around the pyridine to obtain a more dynamic structure and the two α -carboxyl groups in the BDCP^{5-} ligand play a structure-oriented role, causing the other carboxyl groups to grab other metal ions to form binuclear or polynuclear metal-cluster nodes, **NUC-56** possesses excellent characteristics.

From a topological viewpoint, with BDCP^{5-} and $\{\text{In}_2\text{Tm}_2\}$ SBUs being seen as 4 and 8-c nodes, respectively, **NUC-56** can be simplified as a novel 3D (4-c) $_2$ (8-c) topology with the Schläfli symbol of $\{4^{12}\cdot 6^{12}\cdot 8^4\}\{4^6\}_2$ analyzed by TOPOS40, as shown in Fig. 1b.

Analysis of physicochemical properties

As shown in Fig. S2,[†] the PXRD pattern of **NUC-56** and the simulated pattern derived from the single-crystal X-ray data are consistent, proving its phase purity. In addition, the PXRD modes show that **NUC-56** has high water and chemical stability, which was proved by soaking it in water for 7 days at room temperature, 72 h in boiling water, and 7 h in water with a pH in the range of 2 to 12, as shown in Fig. S6 and S7.[†] The

thermal stability of the as-prepared **NUC-56** and **NUC-56a** samples was tested through thermogravimetric analysis experiment (TGA) in the temperature range of 25–800 °C (Fig. S5[†]), which showed a weight loss of ~5.4% (calcd 5.0%) from 25 °C to 100 °C, corresponding to the loss of free H_2O molecules. Next, the second loss of ~23.5% (calcd 22.0%) corresponded to the loss of solvent and associated H_2O molecules from 100 °C to 400 °C. Finally, **NUC-56** was stable up to 450 °C with insignificant further weight loss observed, demonstrating its outstanding thermal stability.

Gas adsorption behaviour

To measure the permanent porosity of **NUC-56a**, the newly-synthesized compound was firstly activated by immersing it in CH_3OH solvent for 3 days, and then heated under dynamic vacuum at 150 °C for 12 h, resulting in the de-solvated **NUC-56a** with abundant open metal active sites on the inner wall of its porous channels. Notably, the skeleton of the activated sample could still maintain its excellent integrity, which is supported by the PXRD pattern (Fig. S4[†]). The N_2 adsorption isotherms of **NUC-56a** were measured at 77 K, as shown in Fig. S8.[†] The obtained results exhibited that **NUC-56a** exhibited the reversible classical Type-I isotherm, confirming that **NUC-56** had microporous characteristics. The BET and

Langmuir surface area were $807 \text{ m}^2 \text{ g}^{-1}$ and $914 \text{ m}^2 \text{ g}^{-1}$, respectively. Furthermore, the aperture distribution measurement showed that its pore size ranged from 8.1 to 14.3 \AA , which illustrates that there were inhomogeneous micro-porous channels in the framework (Fig. S9†).^{53–55} Furthermore, **NUC-56a** also offered the maximum uptake capacity of CO_2 with a value of $90.8 \text{ cm}^3 \text{ g}^{-1}$ at 273 K and $53.5 \text{ cm}^3 \text{ g}^{-1}$ at 298 K (Fig. S10†). To explain the binding force between CO_2 and **NUC-56a**, the isosteric heat of CO_2 adsorption (Q_{st}) determined from the Clausius–Clapeyron equation was calculated to be 28.2 kJ mol^{-1} at zero loading (Fig. S11†).^{56–59}

The distribution of acidic and basic sites in the **NUC-56** catalyst was evaluated by TPD (temperature-programmed desorption) technology, as shown in Fig. 2. In the NH_3 -TPD profile, three groups of ammonia desorption peaks appeared in the temperature range of 100–450 °C, indicating that the NH_3 desorption is from the Lewis acid sites.^{60,61} According to the amount of ammonia desorbed (the integral area of NH_3 -TPD), it is obvious that the amount of stronger Lewis acid sites is greater than weak Lewis basic sites (Fig. 2a). Similarly, it can be seen from the CO_2 -TPD profile in Fig. 2b that Lewis basic sites also exist on the surface of the **NUC-56** catalyst. Also, the number of stronger basic sites is larger than that of weaker basic sites. The TPD results indicate that Lewis acid–base sites exist on the surface of **NUC-56** simultaneously, which is helpful to improve its catalytic performance.

Catalytic cycloaddition of CO_2 and epoxides

Motivated by the features of **NUC-56a** including high stability, large CO_2 sorption capacity, accessible microporous channels, and coexisting high-density Lewis acid and base sites (In^{3+} and Ln^{3+} , $\text{N}_{\text{pyridine}}$ atoms and $\mu_2\text{-OH}$ groups), its heterogeneous catalysis of the cycloaddition reaction was evaluated by using styrene oxide (SO) as a model substrate under solvent-free and mild conditions. Further studies on the reaction temperature, time and catalyst dosage were carried out to optimize the reaction conditions. As described in Table 1, only a few of the reac-

Table 1 Cycloaddition reaction of CO_2 with styrene oxide under various conditions^a

Entry	NUC-56a (mol%)	<i>n</i> -Bu ₄ NBr (mol%)	Temp. (°C)	Time (h)	Yield ^b (%)
1	0.05	0	rt	48	7
2	0	1	rt	48	5
3	0.05	1	rt	48	23
4	0.05	1	35	48	39
5	0.05	1	45	48	66
6	0.05	1	55	48	89
7	0.05	1	65	48	96
8	0.05	2	65	48	99
9	0.05	3	65	36	87
10	0.05	4	65	24	92
11	0.05	5	65	12	95
12	0.06	5	65	12	96
13	0.07	5	65	12	98
14	0.08	5	65	10	97
15	0.09	5	65	8	96
16	0.10	5	65	7	98
17	0.10	0	65	7	58
18	0	5	65	7	43

^a Reaction conditions: 20 mmol styrene oxide, solvent free, CO_2 (1 atm). ^b The *n*-dodecane was internal standard and checked by ¹H NMR and GC-MS spectroscopy.

tion substrates could be converted to the target product at 7% yield in the presence of 0.05 mol% **NUC-56a** at ambient temperature. In contrast, 5% yield was observed when only 1 mol% co-catalyst of *n*-Bu₄NBr as a catalyst was introduced for the cycloaddition reaction, as shown in entry 2. However, when 0.05 mol% of **NUC-56a** and 1 mol% of co-catalyst of *n*-Bu₄NBr were introduced in the cycloaddition reaction under the same reaction conditions, the product yield significantly increased to 23%, indicating that the cycloaddition reaction was

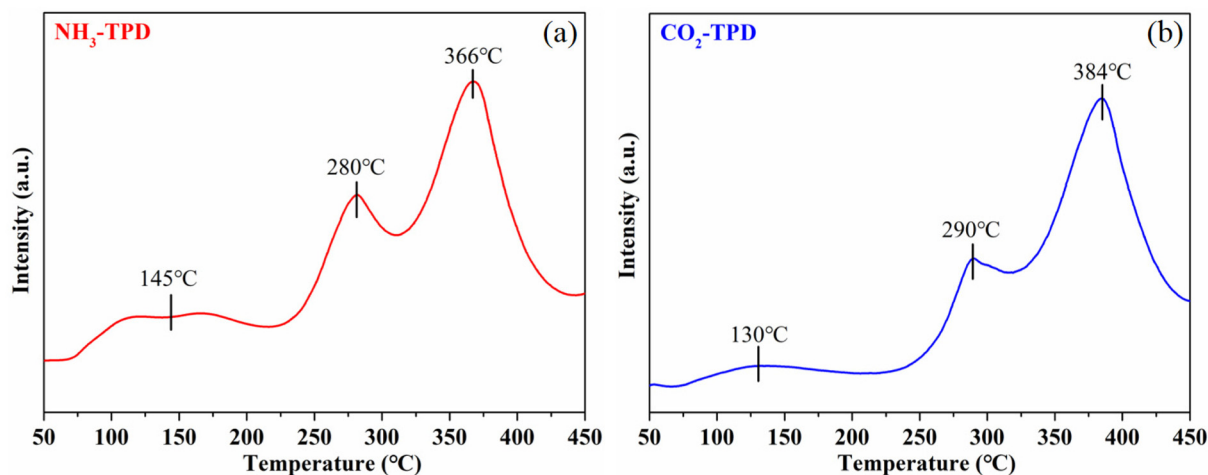


Fig. 2 NH_3 -TPD (a) and CO_2 -TPD (b) profiles of **NUC-56**.

completed by the synergistic catalysis of **NUC-56a** and *n*-Bu₄NBr (entry 3). Besides, with an increase in temperature, the conversion rate increased rapidly with high yield, and when the temperature reached 65 °C, the yield of styrene carbonate (SC) reached 96%, implying that the optimum reaction temperature should be set at 65 °C (entries 4–7). Furthermore, the influence of *n*-Bu₄NBr dosage on the SC yield was investigated. As shown in entries 8–11, as the amount of co-catalyst *n*-Bu₄NBr increased from 1 mol% to 5 mol%, the time taken to produce almost the same yield of SC gradually decreased from 48 h to 12 h. Consequently, the influence of **NUC-56a** dosage was discussed, and the data exhibited that the reaction time was reduced from 12 h to 7 h with the **NUC-56a** dosage from 0.06 to 0.10 mol%, exhibiting that the amount of catalyst has a significant influence on the reaction rate (entries 12–16). In addition, a set of control experiments conducted at 65 °C for 7 h using only 5.0 mol% *n*-Bu₄NBr or 0.10 mol% **NUC-56a** as a new catalytic system exhibited a significant reduction in yield, indicating that the combination of **NUC-56a** and *n*-Bu₄NBr played a very important role in the catalytic process (entries 17 and 18). Thus, it was concluded from the above investigations that the optimum catalytic conditions are 0.10 mol% **NUC-56a**, 5 mol% *n*-Bu₄NBr, 1 atm CO₂, 65 °C and 7 h. As shown in Table S3,† compared with some reports on MOF-based catalytic systems, it is noteworthy that the combination of **NUC-56a** and *n*-Bu₄NBr showed an excellent catalytic effect due to the structural advantages of **NUC-56a**, including high CO₂ adsorption capacity, plentiful Lewis acid and base sites and stable structure.

Inspired by the high catalytic efficiency of **NUC-56a**, epoxides with different substituents were selected to investigate the catalytic universality and size-selectivity under the optimal reaction conditions. As summarized in Table 2, all the selected epoxides with different electronic effects and distinctive steric hindrance were favorably transformed into the corresponding cyclic carbonates with a yield of more than 96%, which were certified by ¹H NMR spectroscopy (Fig. S12–19†). Apparently, the epoxides with strong electron-withdrawing groups (–F, –CF₃, –Cl, and –C=C) and small steric hindrance were almost entirely converted to the desired products because they could contact the reaction active sites without hindrance and electron-withdrawing groups caused a reduction in the electron density of oxygen atoms, which facilitated the critical step of ring opening (Table 2, entries 1–4 and 6).^{62,63} For entries 5 and 7, although the product molecules of 2-ethyloxirane and oxiran-2-ylmethanol had a smaller size than the channel widow of **NUC-56a**, the yield still decreased slightly, which can be attributed to the fact that the substituent groups possessed a notable electron-donating feature.^{64,65} However, the slightly lower yield of styrene carbonate proved that the microporous windows of **NUC-56a** had extremely adverse effects on the large-scale transport of large substrate molecules, reflecting that styrene oxide could not be efficiently reactivated in the catalytic sites.⁶⁶

The recyclability and heterogeneity of a heterogeneous catalyst are key factors for its practical application in organic syn-

Table 2 The cycloaddition reactions of CO₂ with various epoxides with **NUC-56a** as the catalyst^a

E. ^b	Epoxides	Products	Yield ^c (%)	TOF ^d	TON ^e
1			99	142	990
2			99	141	990
3			99	141	990
4			98	140	980
5			97	138	970
6			98	140	980
7			97	138	970
8			96	137	960

^a Reaction conditions: substrate (20 mmol), *n*-Bu₄NBr (5 mol%), **NUC-56a** catalyst (0.10 mol%, based on the active {In₂Tm₂} cluster), CO₂ (1 atm), 65 °C, 7 h. ^bE.: Entry. ^cThe internal standard was *n*-dodecane and checked by GC-MS spectroscopy. ^dTOF = turnover frequency. ^eTON (turnover number) = mole of product/mole of catalyst.

thesis, which prompted us to perform hot leaching and recycling experiments using **NUC-56a** under the optimum conditions. Primarily, the **NUC-56a** catalyst involved in the model reaction was removed by centrifugation after 3 h. The observed SC yield of 63.0% did not change significantly as the reaction time was extended, indicating that **NUC-56a** did not liberate the metal cations and possessed typical heterogeneity (Fig. S23†). Subsequently, the recyclability of **NUC-56a** was evaluated in ten cycle experiments. After each reaction, **NUC-56a** was recovered by centrifugation, washed with strongly polar DMF solvent and the volatile acetone solvent, and dried under vacuum at 120 °C for 5 h. Subsequently, the recovered **NUC-56a** was reused for the next run in the same case. As depicted in Fig. 3, the tenth run gave the yield of SC of 95% with the selectivity remaining over 97%, proving that **NUC-56a** possessed outstanding catalytic ability and superior recoverability. The PXRD and FT-IR profiles of the recycled catalyst used for 10 times were in accordance with the freshly synthesized catalyst. However, there was no significant change in the N₂ adsorption–desorption isotherms, confirming the good stability during the reactions (Fig. S20–S22†). Also, the filtrate

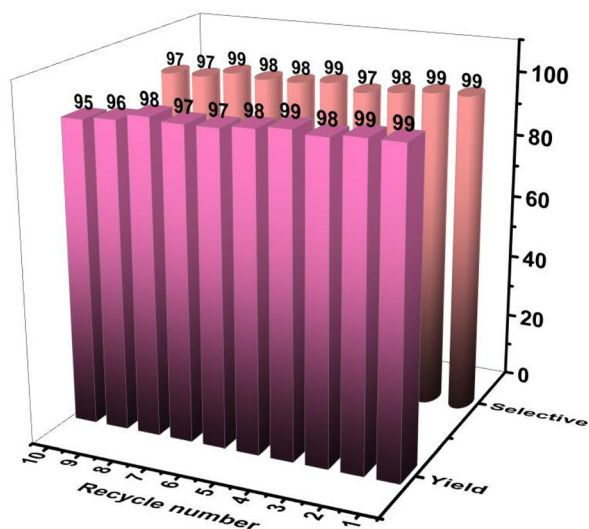


Fig. 3 Recyclability study for catalytic activities of NUC-56a in cycloaddition reaction.

obtained after removing the catalyst was tested by ICP-OES (inductively coupled plasma atomic emission spectrometry) technology, which displayed a negligible quantity of In^{3+} (0.020%) and Tm^{3+} (0.024%) (Table S5[†]). Thus, the above-mentioned results suggest that NUC-56a is an extremely stable and highly efficient heterogeneous catalyst in the field of chemical fixation CO_2 , and has great application prospects.

Therefore, based on the relevant references combined with the excellent characterization and catalytic performance of NUC-56a, the plausible catalytic mechanism for the cycloaddition is exhibited in Fig. 4.^{67–71} Firstly, the cycloaddition reaction began with the O atom of epoxide being activated by the Lewis acidic In^{3+} and Tm^{3+} sites to form In/Tm-epoxide adducts, resulting in the instability of the ternary rings. Subsequently, the Br^- ions released from the co-catalyst of $n\text{-Bu}_4\text{NBr}$ launched an affinity attack on the C atom with less

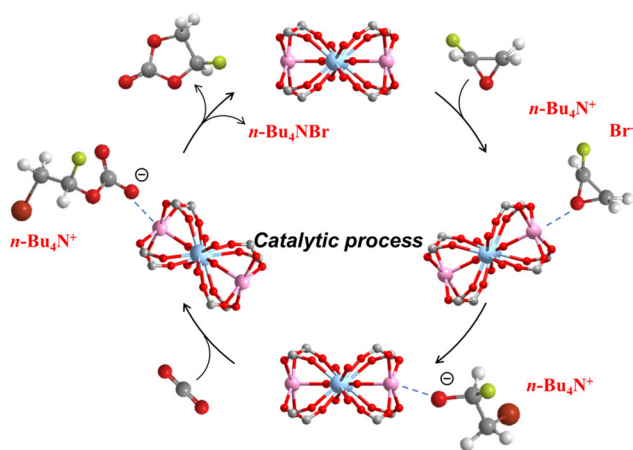


Fig. 4 Proposed reaction mechanism of catalytic cycloaddition reaction.

steric hindrance to produce the main intermediates of alkyl-carbonate anions, whose O^- atoms served as a nucleophilic reagent to react with CO_2 in the pores, generating the carbonate ester as the secondary intermediate. Finally, a closed-loop process was performed to end the reaction, accompanied by the release of NUC-56a and Br^- to participate in the next reaction process.

Catalytic activity of NUC-56a on Knoevenagel condensation

Benefiting from the large number of open Lewis acid–base sites of In^{3+} , Tm^{3+} , $\text{N}_{\text{pyridine}}$ atoms and $\mu_2\text{-OH}$ groups in its nanoporous channels, NUC-56a, as a perfect bifunctional heterogeneous catalyst, could be implemented to catalyze Knoevenagel condensation. As shown in Table 3, in a typical catalytic reaction, benzaldehyde and malononitrile were both introduced in a flask and slowly stirred for 36 h at room temperature under the condition of no NUC-56a. Consequently, the reaction process was continuously monitored by thin layer chromatography (TLC), and only 2% yield was obtained after 36 h, proving that the catalytic reaction hardly occurred the without NUC-56a catalyst, which could be seen as the blank control group for comparison with entry 2. Subsequently, 0.1 mol% NUC-56a was introduced as the catalyst with all the other conditions the same (entry 2). Surprisingly, it was found that the yield of 2-benzylidenemalononitrile in entry 2 (29%) was significantly higher than entry 1, indicating that NUC-56a had a certain promotion effect on the Knoevenagel condensation reaction. In addition, as revealed in entries 2–6, the effect of temperature on the reaction was gradually explored by increments of 10 °C, and the yield reached 99% when the Knoevenagel condensation reaction occurred at 65 °C. Setting 65 °C as the optimal reaction temperature, the influencing factor of the dose of NUC-56a on the reaction was further evaluated. As shown in entries 6–9, when the dose range of

Table 3 Schematic sketch of Knoevenagel condensation using substrates of benzaldehyde and malononitrile^a

Entry	NUC-56a (mol%)	Time (h)	T (°C)	Yield ^b (%)
1	0	36	25	2
2	0.1	36	25	29
3	0.1	36	35	47
4	0.1	36	45	72
5	0.1	36	55	93
6	0.1	36	65	99
7	0.2	24	65	99
8	0.3	12	65	98
9	0.4	8	65	99
10	0.4	2	65	67
11	0.4	4	65	92
12	0.4	6	65	98

^a Reaction conditions: malononitrile (20 mmol), benzaldehyde (10 mmol), ethanol 3 mL. ^b The internal standard was n -dodecane and checked by GC-MS spectroscopy.

NUC-56a increased from 0.1 to 0.4 mol%, the reaction efficiency greatly improved, as evidenced by the high yield obtained in a shorter time. Therefore, the optimal conditions were determined to be 10 mmol benzaldehyde, 20 mmol malononitrile, 0.4 mol% **NUC-56a**, 65 °C and 6 h. Notably, compared with the reported MOFs used as Knoevenagel condensation catalysts, the reaction catalyzed by **NUC-56a** exhibited excellent yield and high TON value, which saved more time and conformed to the principle of green chemistry (Table S6†). Additionally, as illustrated in Fig. S24,† the activating energy of the Knoevenagel condensation reaction calculated using Arrhenius equation was 41.4 kJ mol⁻¹.^{72,73}

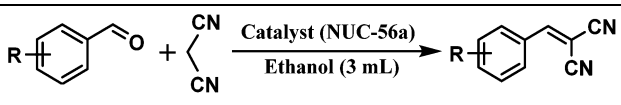
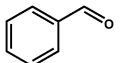
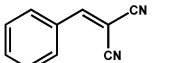
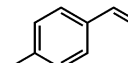
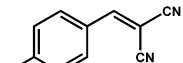
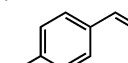
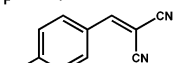
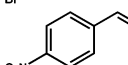
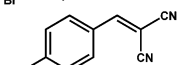
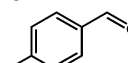
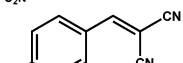
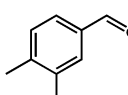
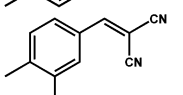
To investigate the effect of different substituents and steric hindrance on the catalytic performance of Knoevenagel condensation, a series of aldehyde derivatives was selected as reactants to carry out the Knoevenagel condensation under the optimal conditions. As shown in entries 2–5 of Table 4, the Knoevenagel condensation reaction of malononitrile with benzaldehyde derivatives substituted with different electron-withdrawing groups (–NO₂, –F and –Br) led to 99% yield, indicating that the electron-withdrawing groups may play a beneficial role in the catalytic process. However, the substrates with electron-donating groups of –CH₃ had a slightly negative impact on the reaction conversion process, showing a decrease in yield (Table 4, entries 5 and 6). Amazingly, the substrate of 3,4-dimethyl benzaldehyde showed an obviously low yield,

which should be attributed to its large molecular size affecting the transport effect of the molecules and the contact opportunity with the reaction sites, as shown in entry 6. All the ¹H NMR spectra of the Knoevenagel condensation products are shown in Fig. S25–S30.†

Moreover, repeatability is an important factor in the practical application of heterogeneous catalysts. After each model reaction of Knoevenagel condensation, **NUC-56a** was separated by centrifugation, washed with DMSO and acetone, and dried under vacuum. As shown in Fig. 5, the recycled **NUC-56a** could maintain its catalytic performance with the yield and selectivity of over 95% even after reuse for ten times. Furthermore, the PXRD profile of **NUC-56a** after ten cycles well matched with the as-synthesized sample, indicating the retention of the initial frame structure during the reaction (Fig. S31†). Alternatively, the FT-IR spectra and the N₂ adsorption–desorption isotherms of the recycled samples used for ten cycles are in accordance with the original crystals, further proving the stability of the reused **NUC-56a** (Fig. S32 and S33†), respectively. Moreover, the supernatant obtained after removing the catalyst was tested by ICP-OES, showing that a negligible quantity of In³⁺ and Tm³⁺ ions leaked from **NUC-56a** (Table S8†). Furthermore, the conducted hot filtration experiments proved that **NUC-56a** owned typical heterogeneity because the model reaction was close to stagnation after removing the catalyst by filtration after 3 h (Fig. S34†).

According to the structural features and composition of **NUC-56a** and the related catalytic systems recorded in the literature, the reaction mechanism of Knoevenagel condensation in the presence of **NUC-56a** was proposed, as shown in Fig. 6.^{74–80} Firstly, the active sites of In³⁺, Tm³⁺, and μ₃-OH ions contact with the O atoms of the aldehyde groups by van der Waals force or hydrogen bonds, weakening the C=O bonds, and then the carbonyl carbon of malononitrile is acti-

Table 4 The Knoevenagel condensation reaction of aldehyde derivatives containing different groups^a

					
E. ^b	Substrate	Products	Yield ^c (%)	TOF ^d	TON ^e
1			99	41	248
2			99	41	248
3			99	41	248
4			99	41	248
5			93	39	234
6			88	36	220

^a Reaction condition: catalyst **NUC-56a** (0.4 mol%, based on the active {In₂Tm₂} cluster), malononitrile (20 mmol), aldehyde derivatives (10 mmol), ethanol 3 mL, 6 h, 65 °C. ^b E.: Entry. ^c Calculation of yield based on GC-MS and ¹H NMR. ^d TOF = turnover frequency. ^e TON (turnover number) = mole of product/mole of catalyst (based on the {In₂Tm₂} cluster).

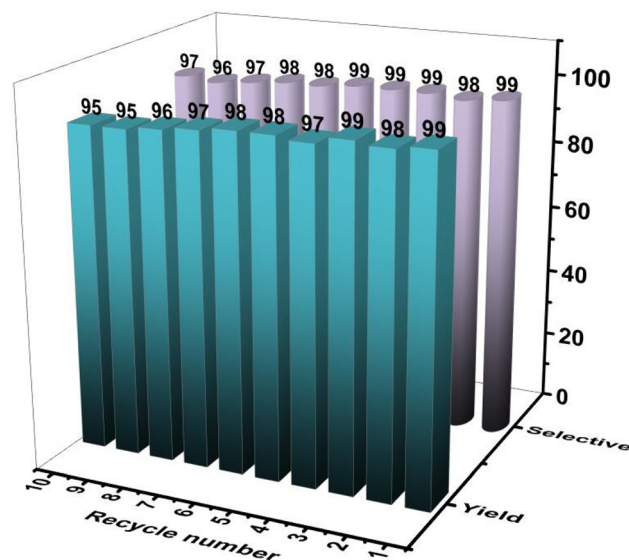


Fig. 5 Recyclability study for catalytic activities of **NUC-56a** in Knoevenagel condensation reaction.

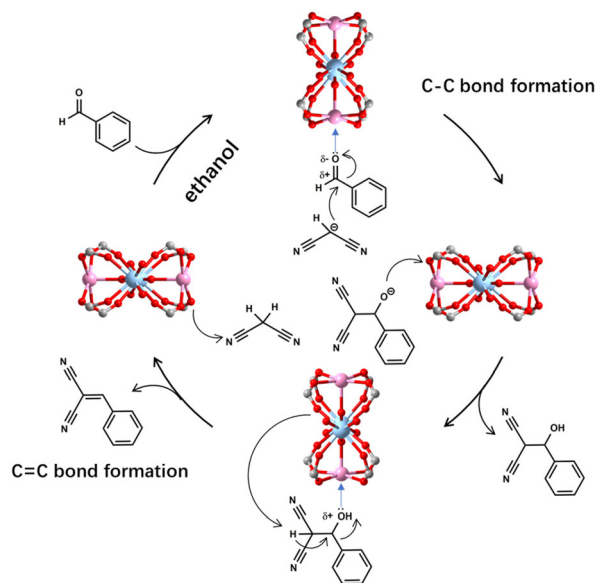


Fig. 6 Proposed reaction mechanism of catalytic Knoevenagel condensation reaction.

vated by the N-pyridine atom to form an active imine intermediate. The imine intermediate tends to undergo a Knoevenagel condensation reaction with the weakened C=O bond of aldehyde. Finally, with the release of water molecules, the product of benzylidenemalonitrile is generated.

Conclusions

The solvothermal self-assembly of In^{3+} , Tm^{3+} and H_5BDCP led to the formation of an extremely stable microporous framework of $\{(\text{Me}_2\text{NH}_2)_2[\text{In}_2\text{Tm}_2(\text{BDCP})_2(\mu_2\text{-OH})_2(\text{H}_2\text{O})_2]\cdot 2\text{DMF}\cdot 3\text{H}_2\text{O}\}_n$ (**NUC-56**) possessing an excellent confined pore environment with large specific surface area, high porosity, and abundant co-existing Lewis acid and base sites of In^{3+} , Tm^{3+} , $\mu_2\text{-OH}$ and $\text{N}_{\text{pyridine}}$ atoms, which are built based on the undocumented heterometallic clusters of $[\text{Tm}_2\text{In}_2(\mu_2\text{-OH})_2(\text{CO}_2)_{10}(\text{H}_2\text{O})_2]$. Due to the excellent characteristics of **NUC-56a**, it showed outstanding stability and excellent catalytic activity for the cycloaddition reactions and Knoevenagel condensation reactions under mild chemical conditions. Thus, this work exhibits that the intervention of high-coordinated rare-earth ions in MOF-based catalysts can realize excellent catalysis, stability and regenerative behaviour, meeting the requirements of long-term stability for the industrial application of these materials.

Author contributions

Hongxiao Lv: conceptualization, writing – original draft, methodology, data curation. Hongtai Chen: formal analysis, investi-

gation. Tuoping Hu: performance testing. Xiutang Zhang: supervision, writing – review & editing, project administration.

Conflicts of interest

All authors express that they have no conflict of interest.

Acknowledgements

The authors thank the National Natural Science Foundation (21101097), Basic Research Program of Shanxi Province (202103021224180), Shanxi Key Laboratory of Advanced Carbon Electrode Materials (202104010910019) and the Opening Foundation of Key Laboratory of Laser & Infrared System of Shandong University (2019-LISKFJJ-005) for funding this work.

References

- 1 X. Liu, L. Xie and Y. Wu, Recent Advances in the Shaping of Metal–organic Frameworks, *Inorg. Chem. Front.*, 2020, **7**, 2840–2866.
- 2 S. Bhattacharjee, S. Bera, R. Das, D. Chakraborty, A. Basu, P. Banerjee, S. Ghosh and A. Bhaumik, A Ni(II) Metal–Organic Framework with Mixed Carboxylate and Bipyridine Ligands for Ultrafast and Selective Sensing of Explosives and Photoelectrochemical Hydrogen Evolution, *ACS Appl. Mater. Interfaces*, 2022, DOI: [10.1021/acsami.2c01647](https://doi.org/10.1021/acsami.2c01647).
- 3 H. Xu, K. Ye, K. Zhu, Y. Gao, J. Yin, J. Yan, G. Wang and D. Cao, Hollow Bimetallic Selenide Derived from a Hierarchical MOF-based Prussian Blue Analogue for Urea Electrolysis, *Inorg. Chem. Front.*, 2021, **8**, 2788–2797.
- 4 K. Berijani and A. Morsali, Photocatalytic Materials: Recent Achievements and Near Future Trends, *Inorg. Chem. Front.*, 2021, **8**, 3618–3658.
- 5 S. V. Dummert, H. Saini, M. Z. Hussain, K. Yadava, K. Jayaramulu and A. Casini, Cyclodextrin Metal–organic Frameworks and Derivatives: Recent Developments and Applications, *Chem. Soc. Rev.*, 2022, **51**, 5175–5213.
- 6 H. Xu, K. Ye, K. Zhu, Y. Gao, J. Yin, J. Yan, G. Wang and D. Cao, Template-directed Assembly of Urchin-like CoSx/Co-MOF as an Efficient Bifunctional Electrocatalyst for Overall Water and Urea Electrolysis, *Inorg. Chem. Front.*, 2020, **7**, 2602–2610.
- 7 X. Zou and Y. Zhang, Noble Metal-free Hydrogen Evolution Catalysts for Water Splitting, *Chem. Soc. Rev.*, 2015, **44**, 5148–5180.
- 8 S. Abednatanzi, P. G. Derakhshandeh, H. Depauw, F. X. Coudert, H. Vrielinck, P. V. D. Voort and K. Leus, Mixed-metal Metal-organic Frameworks, *Chem. Soc. Rev.*, 2019, **48**, 2535–2565.
- 9 Y. B. Huang, J. Liang, X. S. Wang and R. Cao, Multifunctional Metal-organic Framework Catalysts:

- Synergistic Catalysis and Tandem Reactions, *Chem. Soc. Rev.*, 2017, **46**, 126–157.
- 10 L. Chen, H. F. Wang, C. Li and Q. Xu, Bimetallic Metal-organic Frameworks and Their Derivatives, *Chem. Sci.*, 2020, **11**, 5369–5403.
 - 11 Y. Zhao, J. Jing, N. Yan, M. L. Han, G. P. Yang and L. F. Ma, Different Benzendicarboxylate-Directed Structural Variations and Properties of Four New Porous Cd(II)-Pyridyl-Triazole Coordination Polymers, *Inorg. Chem. Front.*, 2020, **8**, 616468.
 - 12 J. Ma, F. Meng, Y. Yu, D. Liu, J. Yan, Y. Zhang, X. Zhang and Q. Jiang, Prevention of Dendrite Growth and Volume Expansion to Give High-performance Aprotic Bimetallic Li-Na Alloy-O₂ Batteries, *Nat. Chem.*, 2019, **11**, 64–70.
 - 13 R. Das, S. S. Dhankhar and C. M. Nagaraja, Construction of a Bifunctional Zn(II)-organic Framework Containing a Basic Amine Functionality for Selective Capture and Room Temperature Fixation of CO₂, *Inorg. Chem. Front.*, 2020, **7**, 72–81.
 - 14 B. Yan, Luminescence Response Mode and Chemical Sensing Mechanism for Lanthanide-functionalized Metal-organic Framework Hybrids, *Inorg. Chem. Front.*, 2021, **8**, 201–233.
 - 15 J. Lan, Y. Qu, Z. Wang, P. Xu and J. Sun, A Facile Fabrication of a Multi-functional and Hierarchical Zn-based MOF as an Efficient Catalyst for CO₂ Fixation at Room-temperature, *Inorg. Chem. Front.*, 2021, **8**, 3085–3095.
 - 16 M. Hu, S. A. A. Razavi, M. Prioozadeh and A. Morsali, Sensing Organic Analytes by Metal-organic Frameworks: a New Way of Considering the Topic, *Inorg. Chem. Front.*, 2020, **7**, 1598–1632.
 - 17 H. Wang, H. Sun, Y. Fu, X. Meng, Y. Zou, Y. He and R. Yang, Varied Proton Conductivity and Photoreduction CO₂ Performance of Isostructural Heterometallic Cluster based Metal-organic Frameworks, *Inorg. Chem. Front.*, 2021, **8**, 4062–4071.
 - 18 Q. Mou, Z. Xu, G. Wang, E. Li, J. Liu, P. Zhao, X. Liu, H. Li and G. Cheng, A Bimetal Hierarchical Layer Structure MOF Grown on Ni Foam as a Bifunctional Catalyst for the OER and HER, *Inorg. Chem. Front.*, 2021, **8**, 2889–2899.
 - 19 M. Ahmed, Recent Advancement in Bimetallic Metal Organic Frameworks (M/MOFs): Synthetic Challenges and Applications, *Inorg. Chem. Front.*, 2022, **9**, 3003–3033.
 - 20 S. Liu, H. Chen and X. Zhang, Bifunctional {Pb₁₀K₂}-Organic Framework for High Catalytic Activity in Cycloaddition of CO₂ with Epoxides and Knoevenagel Condensation, *ACS Catal.*, 2022, **12**(16), 10373–10383.
 - 21 M. Pander, M. Janeta and W. Bury, Quest for an Efficient 2-in-1 MOF-based Catalytic System for Cycloaddition of CO₂ to Epoxides under Mild Conditions, *ACS Appl. Mater. Interfaces*, 2021, **13**, 8344–8352.
 - 22 Z. Gao, L. Liang, X. Zhang, P. Xu and J. Sun, Facile One-pot Synthesis of Zn/Mg-MOF-74 with Unsaturated Coordination Metal Centers for Efficient CO₂ Adsorption and Conversion to Cyclic Carbonates, *ACS Appl. Mater. Interfaces*, 2021, **13**, 61334–61345.
 - 23 Y. Bai, M. Han, X. Li, S. Feng, L. Lu and S. Ma, Facile and Efficient Photocatalyst for Degradation of Chlortetracycline Promoted by H₂O₂, *Inorg. Chem. Front.*, 2022, **9**, 2952–2963.
 - 24 A. J. Kamphuis, F. Picchioni and P. P. Pescarmona, CO₂-fixation into Cyclic and Polymeric Carbonates: Principles and Applications, *Green Chem.*, 2019, **21**, 406–448.
 - 25 L. Jiao, J. Zhu, Y. Zhang, W. Yang, S. Zhou, A. Li, C. Xie, X. Zheng, W. Zhou, S.-H. Yu and H.-L. Jiang, Non-Bonding Interaction of Neighboring Fe and Ni Single-Atom Pairs on MOF-Derived N-Doped Carbon for Enhanced CO₂ Electroreduction, *J. Am. Chem. Soc.*, 2021, **143**, 19417–19424.
 - 26 X. Li, Y. Li, Y. Yang, L. Hou, Y. Wang and Z. Zhu, Efficient Light Hydrocarbon Separation and CO₂ Capture and Conversion in a Stable MOF with Oxalamide-decorated Polar Tubes, *Chem. Commun.*, 2017, **53**, 12970–12973.
 - 27 T. Zhang, H. Chen, S. Liu, H. Lv, X. Zhang and Q. Li, Highly Robust {Ln₄}-organic Frameworks (Ln = Ho, Yb) for Excellent Catalytic Performance on Cycloaddition Reaction of Epoxides with CO₂ and Knoevenagel Condensation, *ACS Catal.*, 2021, **11**, 14916–14925.
 - 28 J. F. Kurisingal, R. Babu, S. Kim, Y. X. Li, J. S. Chang and S. J. Cho, Microwave-induced Synthesis of a Bimetallic Charge-transfer Metal Organic Framework: a Promising Host for the Chemical Fixation of CO₂ via Cyclic Carbonate Synthesis, *Catal. Sci. Technol.*, 2018, **8**, 591–600.
 - 29 V. Aomchad, A. Cristofol, F. D. Monica, B. Limburg, V. D'Elia and A. W. Kleij, Recent Progress in the Catalytic Transformation of Carbon Dioxide into Biosourced Organic Carbonates, *Green Chem.*, 2021, **23**, 1077–1113.
 - 30 C. C. Hou, H. F. Wang, C. Li and Q. Xu, From Metal-organic Frameworks to Single/dual-atom and Cluster Metal Catalysts for Energy Applications, *Energy Environ. Sci.*, 2020, **13**, 1658–1693.
 - 31 S. Liu, H. Chen, H. Lv, Q.-P. Qin, L. Fan and X. Zhang, Chemorobust 4p-5p {InPb}-organic framework for efficiently catalyzing cycloaddition of CO₂ with epoxides and decetalization-Knoevenagel condensation, *Mater. Today Chem.*, 2022, **24**, 100984.
 - 32 C. C. Hou, H. F. Wang, C. Li and Q. Xu, From Metal-organic Frameworks to Single/dual-atom and Cluster Metal Catalysts for Energy Applications, *Energy Environ. Sci.*, 2020, **13**, 1658–1693.
 - 33 B. Parmar, P. Patel, R. S. Pillai, R. K. Tak, R. I. Kureshy, N. H. Khan and E. Suresh, Cycloaddition of CO₂ with an Epoxide Bearing Oxindole Scaffold by a Metal-Organic Framework-Based Heterogeneous Catalyst under Ambient Conditions, *Inorg. Chem.*, 2019, **58**, 10084–10096.
 - 34 S. Zhang, F. Ou, S. Ning and P. Cheng, Polyoxometalate-based Metal-organic Frameworks for Heterogeneous Catalysis, *Inorg. Chem. Front.*, 2021, **8**, 1865–1899.
 - 35 J. Lan, Y. Qu, X. Zhang, H. Ma, P. Xu and J. Sun, A Novel Water-stable MOF Zn(Py)(Atz) as Heterogeneous Catalyst for Chemical Conversion of CO₂ with Various Epoxides under Mild Conditions, *J. CO₂ Util.*, 2020, **35**, 216–224.

- 36 A. K. Ghosh, U. Saha, S. Biswas, Z. A. Allothman, M. A. Islam and M. Dolai, Anthracene-triazole-dicarboxylate-based Zn(II) 2D Metal Organic Frameworks for Efficient Catalytic Carbon Dioxide Fixation into Cyclic Carbonates under Solvent-free Condition and Theoretical Study for the Reaction Mechanism, *Ind. Eng. Chem. Res.*, 2022, **61**, 175–186.
- 37 S. S. Dhankhar and C. M. Nagaraja, Construction of a 3D Porous Co(II) Metal-organic Framework (MOF) with Lewis Acidic Metal Sites Exhibiting Selective CO₂ Capture and Conversion under Mild Conditions, *New J. Chem.*, 2019, **43**, 2163–2170.
- 38 J. Gu, X. Sun, X. Liu, Y. Yuan, H. Shan and Y. Liu, Highly Efficient Synergistic CO₂ Conversion with Epoxide Using Copper Polyhedron-based MOFs with Lewis acid and Base sites, *Inorg. Chem. Front.*, 2020, **7**, 4517–4526.
- 39 R. Das, V. Parihar and C. M. Nagaraja, Strategic Design of a Bifunctional Ag(I)-grafted NHC-MOF for Efficient Chemical Fixation of CO₂ from a Dilute Gas under Ambient Conditions, *Inorg. Chem. Front.*, 2022, **9**, 2583–2593.
- 40 R. Das, T. Ezhil, A. S. Palakkal, D. Muthukumar, R. S. Pillai and C. M. Nagaraja, Efficient Chemical Fixation of CO₂ from Direct Air under Environment-friendly Co-catalyst and Solvent-free Ambient Conditions, *J. Mater. Chem. A*, 2021, **9**, 23127–23139.
- 41 U. Patel, P. Patel, B. Parmar, A. Dadhania and E. Suresh, Synergy of Dual Functional Sites for Conversion of CO₂ in a Cycloaddition Reaction under Solvent-Free Conditions by a Zn(II)-Based Coordination Network with a Ladder Motif, *Cryst. Growth Des.*, 2021, **21**, 1833–1842.
- 42 X.-R. Tian, Y. Shi, S.-L. Hou, Y. Ma and B. Zhao, Efficient Cycloaddition of CO₂ and Aziridines Activated by a Quadruple-Interpenetrated Indium–Organic Framework as a Recyclable Catalyst, *Inorg. Chem.*, 2021, **60**, 15383–15389.
- 43 S. Chong, D. T. Park and J. Kim, Exploring Guest-Dependent Photoconductivity in a Donor-containing Metal–organic Framework, *J. Phys. Chem. C*, 2021, **125**, 10198–10206.
- 44 S. S. Wang, H. H. Huang, M. Liu, S. Yao, S. Guo and J. W. Wang, Encapsulation of Single Iron Sites in a Metal-porphyrin Framework for High-performance Photocatalytic CO₂ reduction, *Inorg. Chem.*, 2020, **59**, 6301–6307.
- 45 Y. H. Li, S. L. Wang, Y. C. Su, K. Bao-Tsan, T. Chen-Yen and C. H. Lin, Microporous 2D Indium Metal-organic Frameworks for Selective CO₂ Capture and their Application in the Catalytic CO₂-cycloaddition of Epoxides, *Dalton Trans.*, 2018, **47**, 9474–9481.
- 46 A. Kong, Q. Lin, C. Mao, X. Bu and P. Feng, Efficient Oxygen Reduction by Nanocomposites of Heterometallic Carbide and Nitrogen-Enriched Carbon Derived from the Cobalt-encapsulated Indium–MOF, *Chem. Commun.*, 2014, **50**, 15619–15622.
- 47 Y. Sun, B. Xia, S. Ding, L. Yu, S. Chen and J. Duan, Rigid Two-Dimensional Indium Metal–organic Frameworks Boosting Nitrogen Electroreduction at all pH Values, *J. Mater. Chem. A*, 2021, **9**, 20040–20047.
- 48 G. Verma, K. Forrest, B. A. Carr, H. Vardhan and S. Ma, Indium–organic Framework with *soc* Topology as a Versatile Catalyst for Highly Efficient One-pot Strecker Synthesis of α -aminonitriles, *ACS Appl. Mater. Interfaces*, 2021, **13**, 52023–52033.
- 49 C. Lu, D. Xiong, C. Chen, J. Wang, Y. Kong, T. Liu, S. Ying and F. Yi, Indium-based Metal–organic Framework for Efficient Photocatalytic Hydrogen Evolution, *Inorg. Chem.*, 2022, **61**, 2587–2594.
- 50 L. Zhai, J. W. Yu, J. Zhang, W. W. Zhang, L. Wang and X. M. Ren, High Quantum Yield Pure Blue Emission and Fast Proton Conduction from an Indium–metal–organic Framework, *Dalton Trans.*, 2019, **48**, 12088–12095.
- 51 Y. Zhang, S. Liu, Z. S. Zhao, Z. Wang, R. Zhang and L. Liu, Recent Progress in Lanthanide Metal–organic Frameworks and Their Derivatives in Catalytic Applications, *Inorg. Chem. Front.*, 2021, **8**, 590–619.
- 52 M. Tian, J. Zheng, J. Xue, X. Pan, D. Zhou and Q. Yao, A Series of Microporous and Robust Ln-mofs Showing Luminescence Properties and Catalytic Performances towards Knoevenagel Reactions, *Dalton Trans.*, 2021, **50**, 17785–17791.
- 53 H. Chen, Z. Zhang, T. Hu and X. Zhang, An NH₂-modified {Eu^{III}}_2-Organic Framework for the Efficient Chemical Fixation of CO₂ and Highly Selective Sensing of 2,4,6-Trinitrophenol, *Inorg. Chem. Front.*, 2021, **8**, 4376–4385.
- 54 R. Babu, R. Roshan, A. C. Kathalikkattil, D. Kim and D. W. Park, Rapid, Microwave-assisted Synthesis of Cubic, Three-dimensional, Highly Porous mof-205 for Room Temperature CO₂ Fixation via Cyclic Carbonates synthesis, *ACS Appl. Mater. Interfaces*, 2016, **8**, 33723–33731.
- 55 P. C. Purba, M. Venkateswaralu, S. Bhattacharyya and P. S. Mukherjee, Silver(I)–Carbene Bond-Directed Rigidification-Induced Emissive Metallacage for Picric Acid Detection, *Inorg. Chem.*, 2022, **61**, 713–722.
- 56 Y. B. N. Tran, P. T. K. Nguyen, Q. T. Luong and K. D. Nguyen, Series of M-MOF-184 (M=Mg, Co, Ni, Zn, Cu, Fe) Metal–Organic Frameworks for Catalysis Cycloaddition of CO₂, *Inorg. Chem.*, 2020, **59**, 16747–16759.
- 57 G. Mercuri, M. Moroni, S. Galli, G. Tuci, G. Giambastiani, T. Yan, D. Liu and A. Rossin, Temperature-dependent Nitrous Oxide/Carbon Dioxide Preferential Adsorption in a Thiazolium-functionalized NU-1000 Metal–organic Framework, *ACS Appl. Mater. Interfaces*, 2021, **13**, 58982–58993.
- 58 W. L. Xue, L. Wang, Y. K. Li, H. Chen and C. Q. Wan, Reticular Chemistry for Ionic Liquid-functionalized Metal–organic Frameworks with High Selectivity for CO₂, *ACS Sustainable Chem. Eng.*, 2020, **8**, 18558–18567.
- 59 Z. Bian, Y. Zhang, D. Tian, X. Zhang, L. Xie, M. Zhao, Y. Xie and J. Li, Co₇-Cluster-Based Metal-organic Frameworks with Mixed Carboxylate and Pyrazolate Ligands: Construction and CO₂ Adsorption and Fixation, *Cryst. Growth Des.*, 2020, **20**, 7972–7978.
- 60 X. Chen, E. Yu, S. Cai, H. Jia, J. Chen and P. Liang, In Situ Pyrolysis of Ce-MOF to Prepare CeO₂ Catalyst with

- Obviously Improved Catalytic Performance for Toluene Combustion, *Chem. Eng. J.*, 2018, **344**, 469–479.
- 61 L. Yang, H. Zhang, P. Tao, X. Lu and Q. Xia, Microwave-assisted Air Epoxidation of Mixed Biolefins over a Spherical Bimetal ZnCo-MOF Catalyst, *ACS Appl. Mater. Interfaces*, 2021, **13**, 8474–8487.
- 62 R. Cao, Z. Chen, Y. Chen, K. B. Idrees, S. L. Hanna, X. Wang, T. A. Goetjen, Q. Sun, T. Islamoglu and O. K. Farha, Benign Integration of a Zn-azolate Metal-organic Framework onto Textile Fiber for Ammonia Capture, *ACS Appl. Mater. Interfaces*, 2020, **12**, 47747–47753.
- 63 D. Chen, W. Yang, L. Jiao, L. Li, S.-H. Yu and H.-L. Jiang, Boosting Catalysis of Pd Nanoparticles in MOFs by Pore Wall Engineering: the Roles of Electron Transfer and Adsorption Energy, *Adv. Mater.*, 2020, **32**, 2000041.
- 64 J. Lan, Y. Qu, Z. Wang, P. Xu and J. Sun, A Facile Fabrication of a Multi-functional and Hierarchical Zn-based MOF as an Efficient Catalyst for CO₂ Fixation at Room-temperature, *Inorg. Chem. Front.*, 2021, **8**, 3085–3095.
- 65 Y. Guo, B. Gao, Z. Deng, Y. Liu, X. Peng and Y. Zhao, Charge Separation in Hybrid Metal-organic Framework Films for Enhanced Catalytic CO₂ conversion, *J. Mater. Chem. A*, 2021, **9**, 2694–2699.
- 66 H. Lv, Z. Zhang, L. Fan, Y. Gao and X. Zhang, A Nanocaged Cadmium-organic Framework with High Catalytic Activity on the Chemical Fixation of CO₂ and Deacetalization-knoevenagel Condensation, *Microporous Mesoporous Mater.*, 2022, **51**, 111791.
- 67 H. Chen, T. Zhang, S. Liu, H. Lv, L. Fan and X. Zhang, Fluorine-Functionalized NbO-Type {Cu₂}-Organic Framework: Enhanced Catalytic Performance on the Cycloaddition Reaction of CO₂ with Epoxides and Deacetalization-Knoevenagel Condensation, *Inorg. Chem.*, 2022, **61**, 11949–11958.
- 68 T. Stolar, A. Pranikar, V. Martinez, B. Karadeniz and K. Uarevi, Scalable Mechanochemical Amorphization of Bimetallic Cu-Zn MOF-74 Catalyst for Selective CO₂ Reduction Reaction to Methanol, *ACS Appl. Mater. Interfaces*, 2021, **13**, 3070–3077.
- 69 F. Ma, F. Mi, M. Sun, T. Huang, Z. Wang, T. Zhang and R. Cao, A Highly Stable Zn₉-pyrazolate Metal-organic Framework with Metallosalen Ligands as a Carbon Dioxide Cycloaddition Catalyst, *Inorg. Chem. Front.*, 2022, **9**, 1812–1818.
- 70 A. Liu, Y. Chen, P. Liu, W. Qi and B. Li, Conversion of CO₂ to Epoxide or Oxazolidinone Enable by a Cu^I/Cu^{II}-organic Frameworks Bearing a tri-functional linker, *Inorg. Chem. Front.*, 2022, **9**, 4425–4432.
- 71 M. Pander, M. Janeta and W. Bury, Quest for an Efficient 2-in-1 MOF-based Catalytic System for Cycloaddition of CO₂ to Epoxides under Mild Conditions, *ACS Appl. Mater. Interfaces*, 2021, **13**, 8344–8352.
- 72 Q. Niu, Y. Wang, G. Li, Y. Zhao, V. Singh, J. Niu and J. Wang, Polyoxoniobates as a Superior Lewis base Efficiently Catalyzed Knoevenagel Condensation, *Mol. Catal.*, 2018, **453**, 93–99.
- 73 Y. Ren, H. Li, W. Yang, D. Shi, Q. Wu, Y. Zhao, C. Feng, H. Liu and Q. Jiao, Alkaline Ionic Liquids Immobilized on Protective Copolymers Coated Magnetic Nanoparticles: an Efficient and Magnetically Recyclable Catalyst for Knoevenagel Condensation, *Ind. Eng. Chem. Res.*, 2019, **58**, 2824–2834.
- 74 A. Das and K. Thomas, Rose Bengal Photocatalyzed Knoevenagel Condensation of Aldehydes and Ketones in Aqueous Medium, *Green Chem.*, 2022, **24**, 4952–4957.
- 75 H. Lv, L. Fan, H. Chen, X. Zhang and Y. Gao, Nanochannel-based {BaZn}-organic Framework for Catalytic Activity on the Cycloaddition Reaction of Epoxides with CO₂ and Deacetalization-knoevenagel condensation, *Dalton Trans.*, 2022, **51**, 3546–3556.
- 76 F. Ghobakhloo, D. Azarifar, M. Mohammadi, H. Keypour and H. Zeynail, Copper(II) Schiff-Base Complex Modified UiO-66-NH₂(Zr) Metal-Organic Framework Catalysts for Knoevenagel Condensation–Michael Addition–Cyclization Reactions, *Inorg. Chem.*, 2022, **61**, 4825–4841.
- 77 J. N. Appaturi, R. Ratti, B. L. Phoon, S. M. Batagarawa, I. Dia, M. Selvaraj and R. J. Ramalingam, Mixed-Linker Isoreticular Zn(II) Metal-Organic Frameworks as Brønsted Acid-Base Bifunctional Catalysts for Knoevenagel Condensation Reactions, *Dalton Trans.*, 2022, **51**, 2567–2576.
- 78 S. Johari, M. R. Johan and N. G. Khaligh, An Overview of Metal-Free Sustainable Nitrogen-based Catalytic Knoevenagel Condensation Reaction, *Org. Biomol. Chem.*, 2022, **20**, 2164–2186.
- 79 J. Qiao, B. Zhang, L. Zhang and Y. Liu, Practice of Function-oriented Synthesis: Efficient CO₂ Conversion and Knoevenagel Condensation by Two New In₃ based MOFs with High-density Active Sites under Mild Conditions, *J. Mater. Chem. A*, 2022, **10**, 17773–17781.
- 80 A. Karmakar, M. M. A. Soliman, G. M. D. M. Rubio, M. F. C. Silva and A. J. L. Pombeiro, Synthesis and Catalytic Activities of a Zn(II) Based Metallomacrocyclic and a Metal-organic Framework towards One-pot Deacetalization-knoevenagel Tandem Reactions under Different Strategies: a Comparative Study, *Dalton Trans.*, 2020, **49**, 8075–8085.